COMPUTATIONAL STUDIES OF MOLECULAR PERMEATION THROUGH CONNEXIN26 CHANNELS

Supporting Material

Yun Luo[1*], Angelo R. Rossi[2], Andrew L. Harris[2]

[1] Pharmaceutical Sciences Department, College of Pharmacy, Western University of Health Sciences, Pomona, CA

[2] Department of Pharmacology, Physiology and Neuroscience, Rutgers New Jersey Medical School, Rutgers University, Newark, NJ

Supporting results

PMFs derived from SMD simulations

In addition to the US/H-REMD simulations, SMD simulations were carried out for the test molecules. For each test molecule, five to eight SMD trajectories of 4 ns each were calculated. For each trajectory, values of the force and coordinates were saved every 0.02 ps for a total of 200,000 points. The trajectories were then divided into time windows of 10 ps, and the mean position of the test molecule in each window was determined. An average was then taken over the time slices, followed by a final average over multiple trajectories (33,34,70-72). This procedure minimizes accumulated error in the calculated work. The division of SMD trajectories into 10 ps time windows yielded 400 blocks of work values for each trajectory. The mean of the block averages, their standard deviation, and their standard error were then calculated. For the disaccharide, this led to a 12.8% standard error of the mean work value. The trisaccharide data had a standard error of 10.1% of the mean work value. The distributions of work values were Gaussian, which indicates that they were not biased by the pulling force.

The PMFs derived from the SMD simulations had some similarity to those derived from US/H-REMD, but differed in significant ways. They showed broad peaks shifted toward the cytoplasmic end of the pore (more negative *z*-positions) relative to the US/H-REMD peaks. More important, the difference between the PMF peaks for the two test molecules is much less than in the US/H-REMD results and do not overtly correlate with a pore narrowing. The difference in the peaks is ~1.25 kcal/mol. If the difference in the peaks defines the relative permeability, the SMD PMFs suggest that the disaccharide is approximately 8-fold more permeable than the trisaccharide. US/H-REMD appears to more accurately capture the forces involved in permeation of these molecules through connexin channels than does SMD. This may be due to several factors, including the non-equilibrium nature of SMD leading to inability to fully capture the forces in the context of highly flexible permeants and a wide pore (73) lined by sidechains that can adopt relatively unconstrained rotamer configurations. Also, the SMD method does not capture the energy that is held and released dissipatively in conformational changes of the test molecules due to the pulling force (54).

van der Waals and Polar Interactions

The van der Waals (vdW) and polar character of the interactions of the test molecules within the pore were explored. The results indicate that the vdW interactions of the test molecules with water and protein are strong and favorable throughout the pore, often with reciprocal changes regarding interaction with water and with protein (Figure S8). This indicates that the protein and water molecules compete in forming favorable vdW contacts with the test molecules throughout the permeation process. The calculation of polar interactions results suggest that in the region between z = 2 Å and z = 15 Å there may be favorable electrostatic interactions with the trisaccharide that do not occur for the disaccharide (Figure S9). As noted in Methods, the calculated magnitude of the polar interaction is strongly dependent on the chosen value of dielectric constant (ε = 20 in Figure S9), a concept that is difficult to apply within a pore, so one cannot determine from this calculation the degree to which polar interactions contribute to the PMF. However, the results do identify a region of the pore at which there are opportunities for significant polar interactions. Such interactions may not be energetically significant for the

uncharged test molecules used here, but would be expected to be much more significant for charged or zwitterionic molecules of similar size.

Interaction with Water

In ion-specific channels, energetic compensation for loss of solvating water is a key factor in selectivity. The number of water molecules within 5 Å (roughly the first solvent shell) of the test molecules was determined (Figure S12). For the disaccharide, the only notable change in closely associated water within the pore is a modest increase between z = 15 and 30 Å. The trisaccharide shows greater fluctuations in the number of associated waters but little overall change. In spite of the variations, there is no indication of significant dehydration. However, the results suggest a substantial cloud of associated water molecules, which may be directly hydrogen bonded to the test molecules, may contribute to the effective hydrodynamic radius of the molecules and thereby viscous drag (i.e., intrapore diffusion).

Supporting Figures

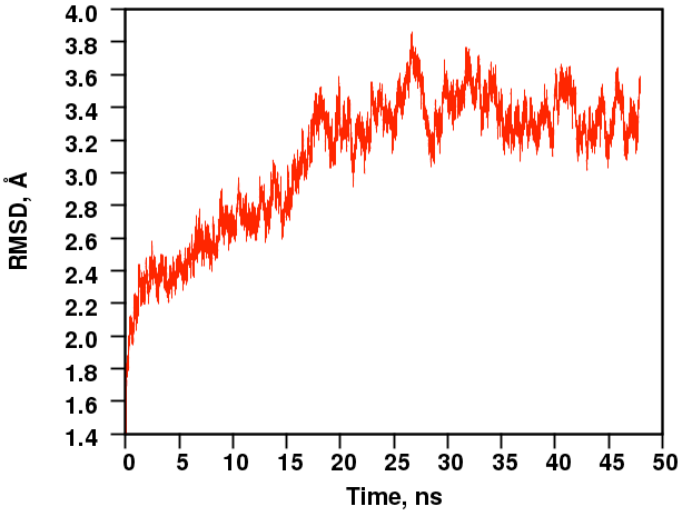

Figure S1: RMSD of the Cx26 channel heavy atoms during 50 ns of dynamics.

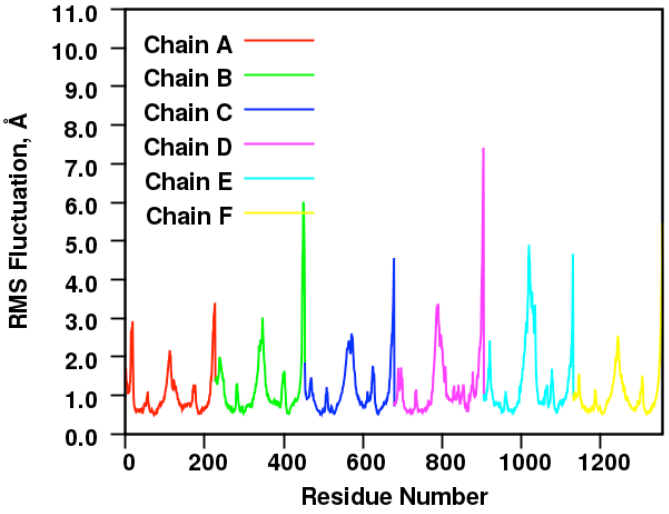

Figure S2: RMSF of equilibrated Cx26 channel as a function of sequential residue number. Each connexin monomer composing the hexameric channel is depicted in a different color. The peaks at the beginning and end of each connexin monomer correspond to part of the N-terminal domain (NT) and to the cytoplasmic C-terminal domain (CT), respectively. The major peak in the middle of each monomer corresponds to residue R104 in the cytoplasmic loop domain. The minor peaks on either side of the R104 peaks correspond to E47 and G160 in the extracellular loops.

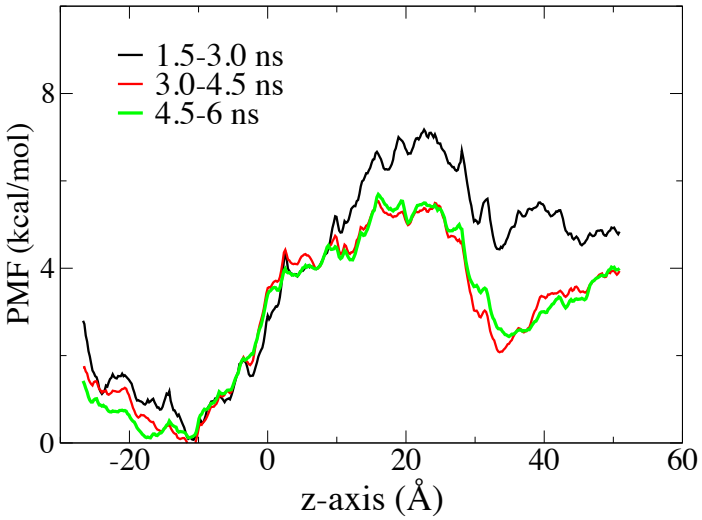

Figure S3: Convergence of the US/H-REMD PMFs for the disaccharide. The simulation time per replica is indicated.

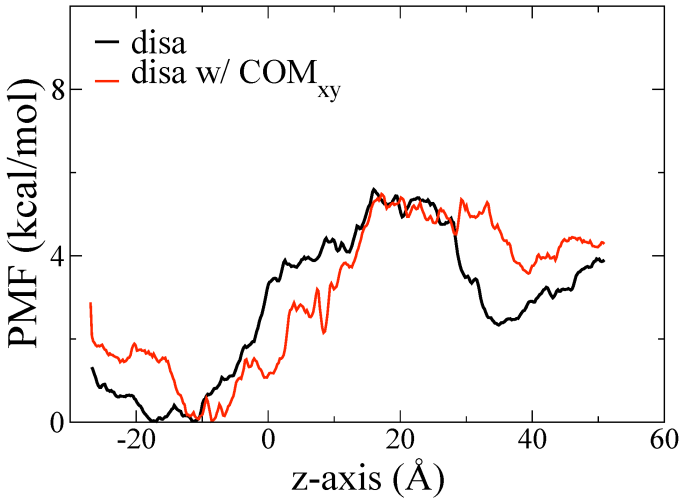

Figure S4: Comparison of disaccharide US/H-REMD PMFs computed with and without COM_{xy} restraint.

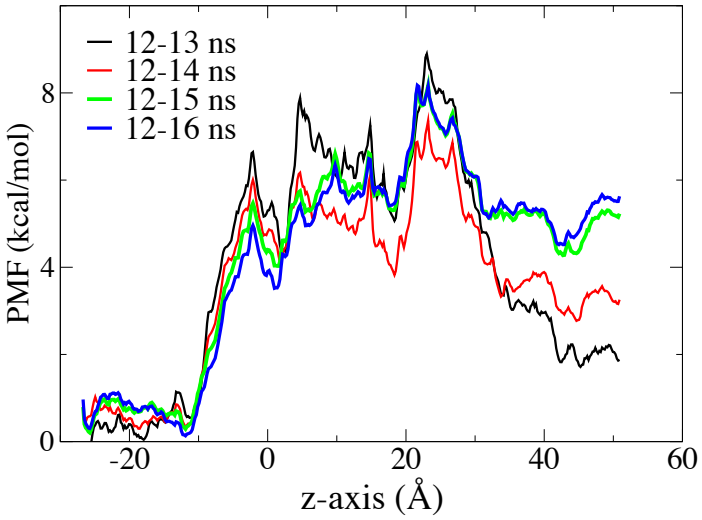

Figure S5: Convergence of the US/H-REMD PMFs for the trisaccharide, with COM_{xy} restraint. The simulation time per replica is indicated.

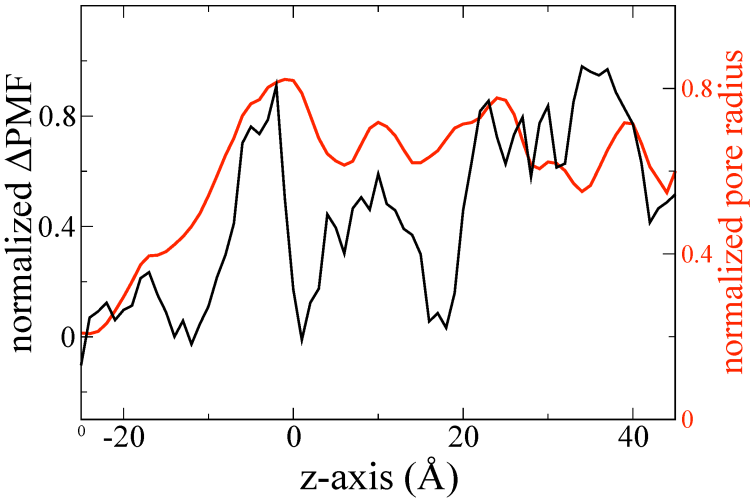

Figure S6: Normalized ΔPMF ($PMF_{trisaccharide} - PMF_{disaccharide}$) from US/H-REMD simulations (black), and normalized pore width (narrower toward the top; red).

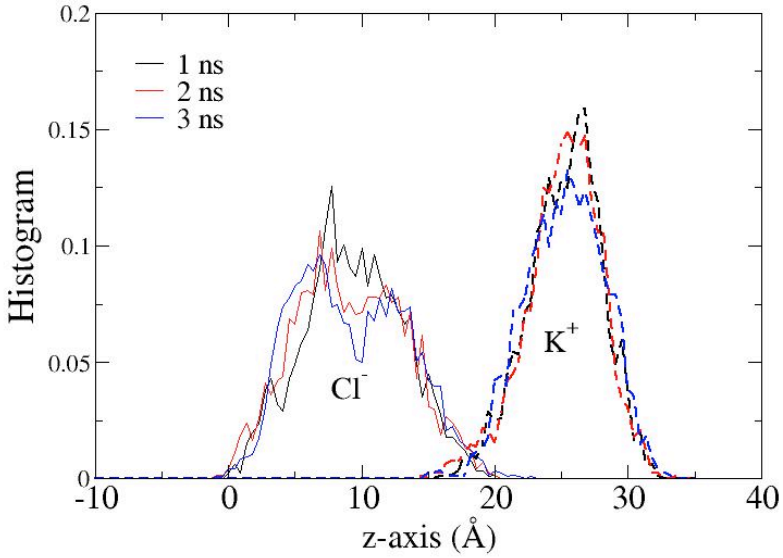

Figure S7: Distribution of chloride ions (solid lines) and potassium ions (dashed lines) along *z*-axis inside the Cx26 channel from US/H-REMD simulations. Different colors indicate the simulation time.

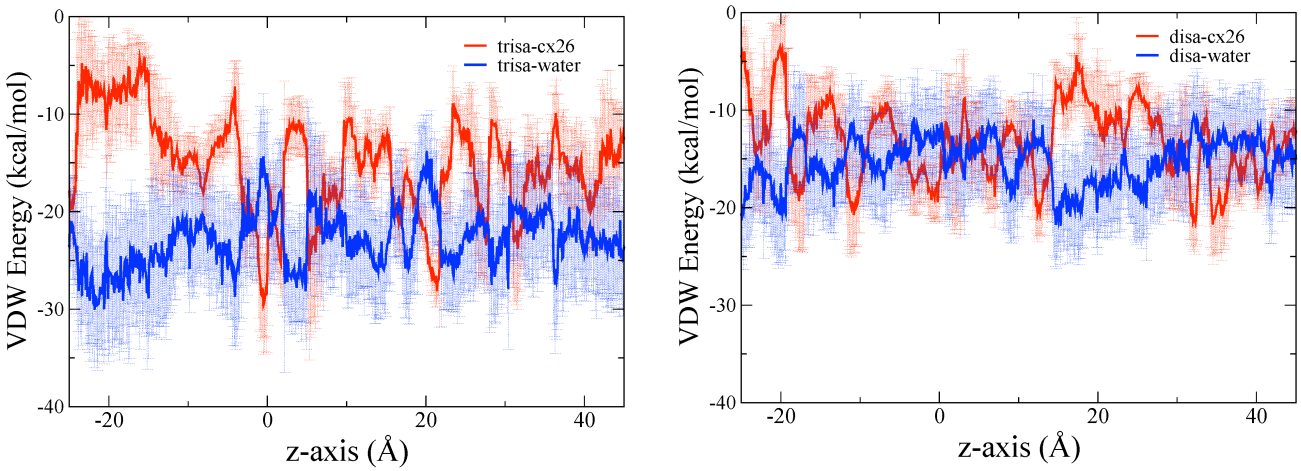

Figure S8: van der Waals interaction energies between the test molecules and the connexin protein from US/H-REMD simulations. Similar to the force decomposition (Figure 3), the results show essentially reciprocal energy relationships of the test molecules with the Cx26 protein and water within the pore. The most favorable Lennard-Jones interaction between water and disaccharide is between z positions 15 and 30 Å, corresponding to a broad but modest peak in the number of waters within 5 Å (Figure S12). The trisaccharide shows less favorable Lennard-Jones interaction with water at narrow regions at $z \approx 0$ Å and $z \approx 20$ Å, which may correlate with some loss of close water (Figure S12).

Figure S9: Normalized polar interaction energies between the test molecules and the connexin protein (Note: The magnitude of the calculated polar energy is a function of the chosen dielectric, so the curves only indicate regions of the pore at which polar interactions may be significant, and where they differ for the two molecules).

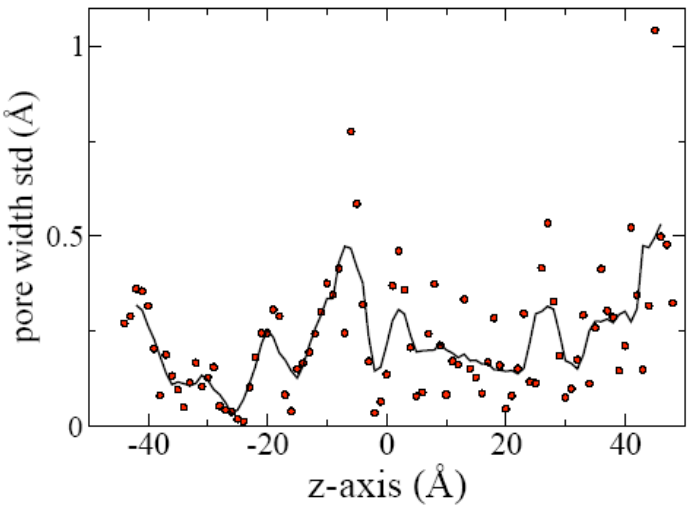

Figure S10: Standard deviation of the pore width, and a trendline (rolling average).

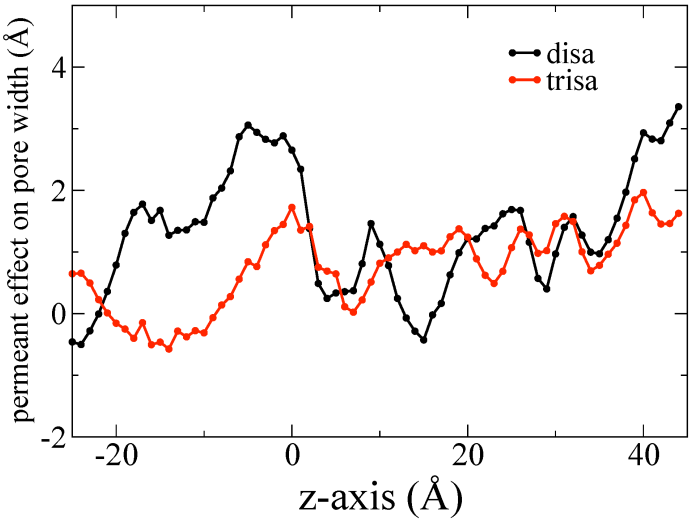

Figure S11: Effect of each test molecule on width of the pore at the *z*-position of the molecule, relative to width of unoccupied pore. Disaccharide: black; Trisaccharide: red

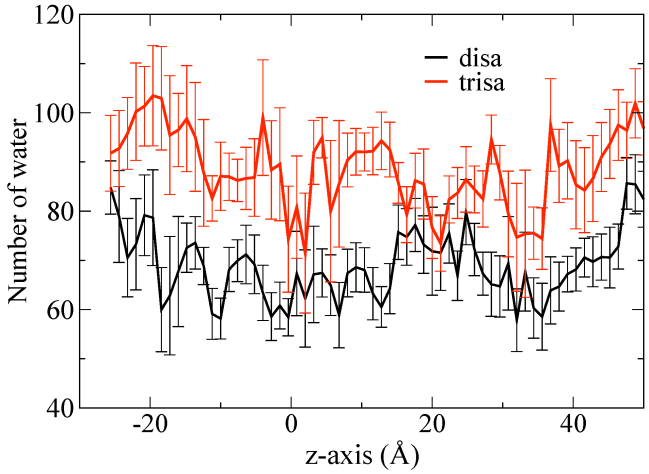

Figure S12: Number of water molecules within 5 Å of the test molecules from US/H-REMD simulations. Error bars are standard deviations.

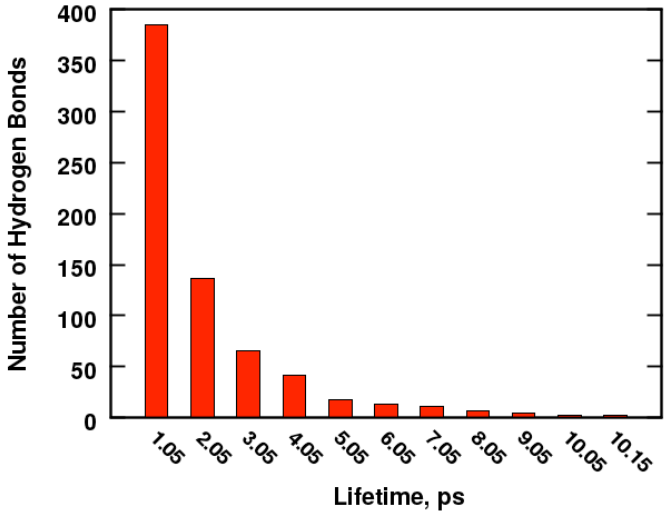

Figure S13: Histogram of lifetimes of hydrogen bonds between disaccharide and water.

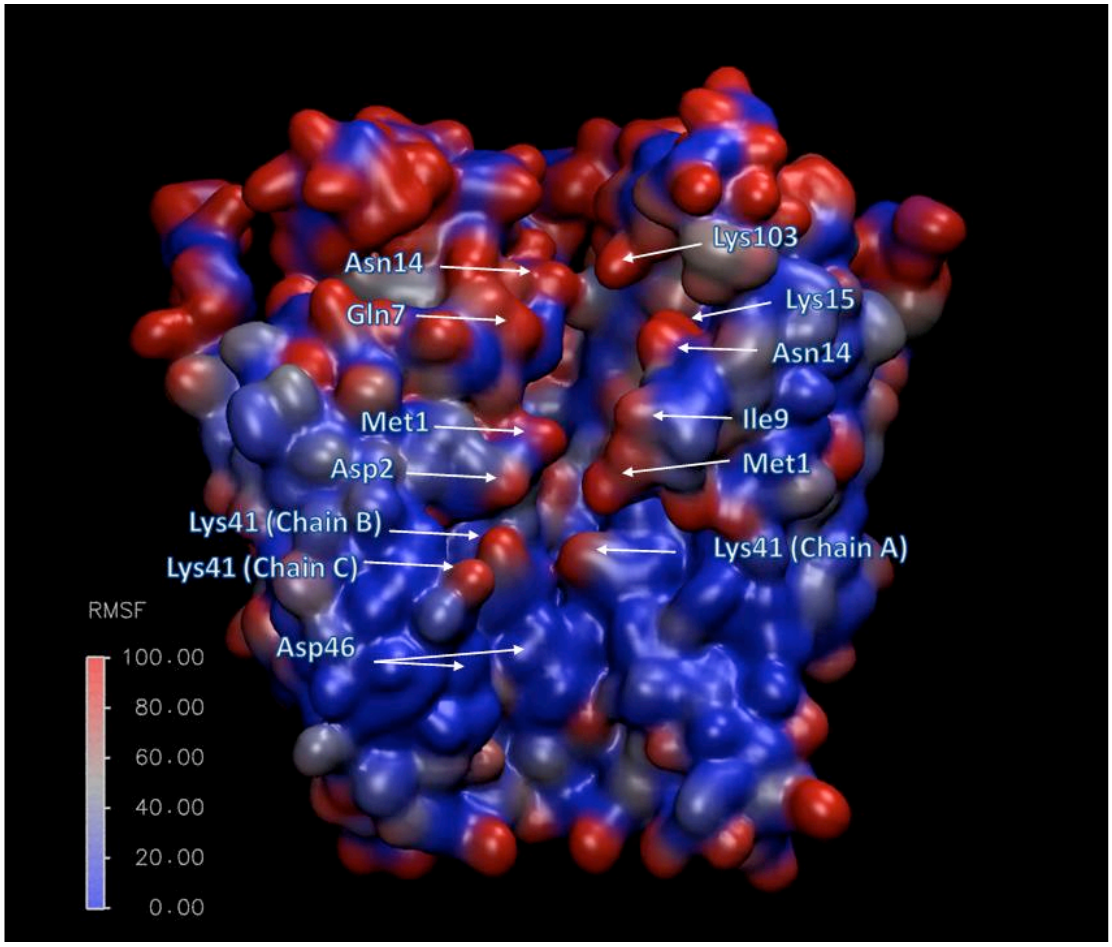

Figure S14: Cutaway of the channel color-coded by per-sidechain RMSF values. The channel is depicted in a single snapshot during the US/H-REMD simulations, with 3 of the connexin subunits removed so that the pore can be seen. Note that the residues of the NT domain (residues 1-15) and in particular MET1 and ASP2 (which roughly correspond to the narrow region around z = -2 Å) and LYS41 (which corresponds to a secondary narrow region at z = 10 Å) have high RMSF values. In contrast, the ASP46 residue, which corresponds to the peak of the PMF, is relatively rigid.

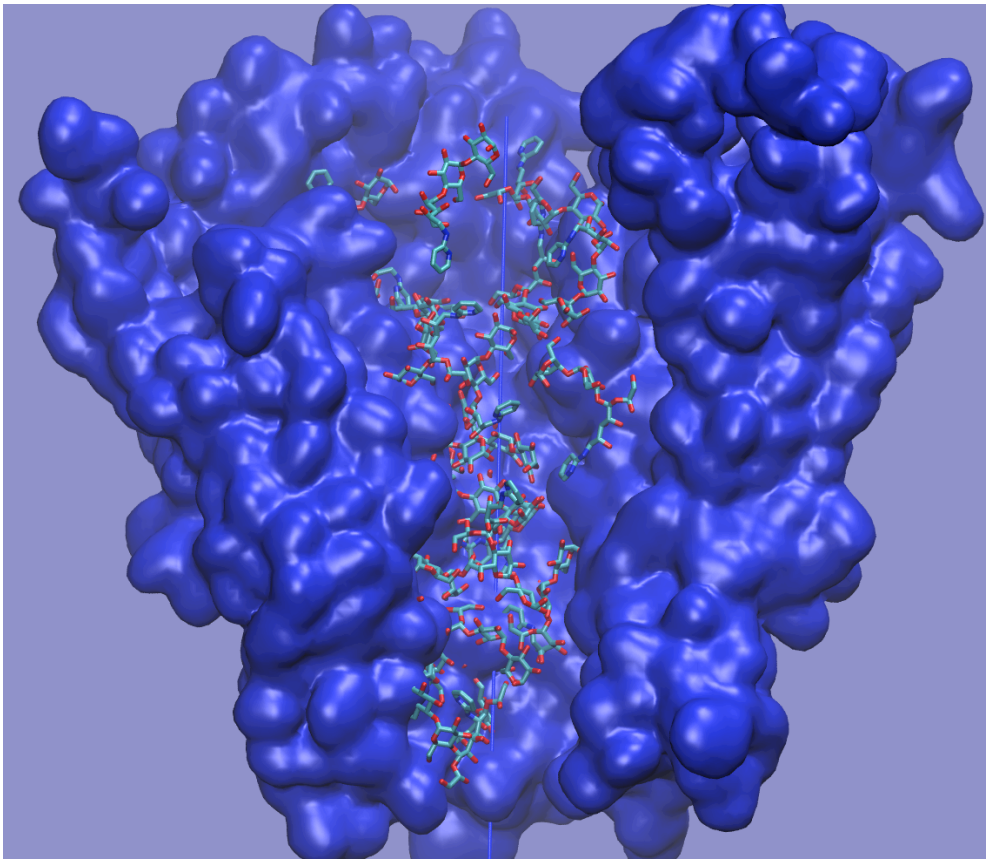

Figure S15: Path of the trisaccharide through the channel during a US/H-REMD simulation (without COM_{xy} restraint). The image depicts overlapped snapshots of the trisaccharide at 1 ns interval.

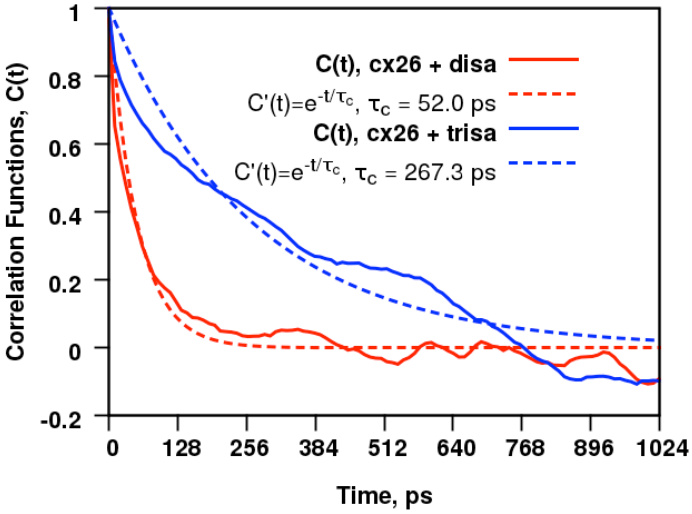

Figure S16: Autocorrelation functions of test molecule radius of gyration within the pore.

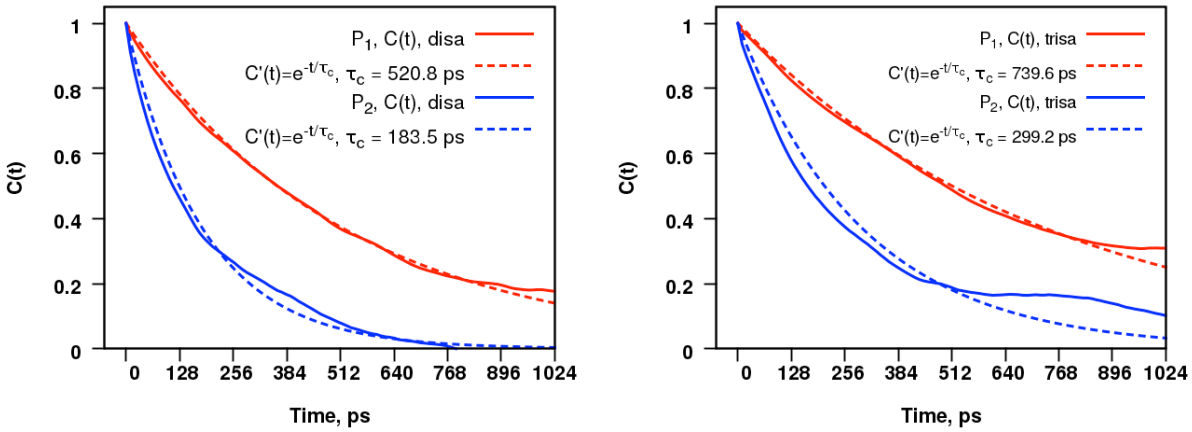

Figure S17: Autocorrelation functions of test molecule rotation within the pore.

Supporting Table: Hydrogen bond position and occupancy.

z (backbone atom)	z (sidechain atom)	Cx26-disa (residue, occupancy)	Cx26-water-disa (residue, occupancy)	DISA sidechain/ backbone	DISA occupancy	Cx26-trisa (residue, occupancy)	Cx26-water-trisa (residue, occupancy)	TRISA sidechain/ backbone	TRISA occupancy
-0.1 (1.0)	0.6 (1.5)	ASP2 0.38	ASP2 0.49	**12.1/1**	**.870***	ASP2 0.133	ASP2 0.49	**2.9/1**	**.623***
-1.0 (1.2)	0.7 (1.1)						TRP3 0.08	**1.6/1**	**.080**
-3.0 (1.3)		GLY4 0.054	GLY4 0.105	**backbone**	**.159**	GLY4 0.064	GLY4 0.10	**backbone**	**.164**
-3.6 (1.0)	-1.9 (1.1)		THR5 0.167	**30.2/1**	**.167**	THR5 0.055	THR5 0.17	**124.6/1**	**.225**
-4.4 (1.0)			LEU6 0.0531	**backbone**	**.053**				
-5.5 (1.1)	-4.1 (1.7)		GLN7 0.0978	**14.1/1**	**.098**	GLN7 0.050	GLN7 0.16	**124.6/1**	**.210**
-6.0 (1.0)	-4.2 (1.1)					THR8 0.054	THR8 0.068	**40.1/1**	**.122**
15.4 (0.9)			ALA40 0.0538	**backbone**	**.054**		ALA40 0.068	**backbone**	**.068**
16.1 (1.0)	10.7 (1.2)	LYS41 0.104	LYS41 0.205	**2.5/1**	**.309***	LYS41 0.175	LYS41 0.26	**1.3/1**	**.435***
18.7 (1.0)	14.5 (1.0)						GLU42 0.14	**5.4/1**	**.140**
24.5 (1.0)	23.4 (0.9)	ASP46 0.101	ASP46 0.154	**1.6/1**	**.255***	ASP46 0.158	ASP46 0.38	**2.6/1**	**.538***
	20.6 (0.9)						GLU47 0.05	**sidechain**	**.050**
28.2 (1.0)	27.3 (0.9)						GLN48 0.078	**8.1/1**	**.078**
29.5 (1.0)			ALA49 0.134	**backbone**	**.134**		ALA49 0.16	**backbone**	**.160**
27.2 (0.8)	27.7 (0.5)	ASP50 0.108	ASP50 0.193	**111.0/1**	**.301***	ASP50 0.059	ASP50 0.149	**12.7/1**	**.208**
37.1 (0.9)			CYS53 0.0756	**backbone**	**.076**		CYS53 0.08	**backbone**	**.080**
42.4 (0.8)	41.1 (0.5)						ASN54 0.068	**1/2.3**	**.068**
40.8 (0.7)	41.4 (0.6)		THR55 0.0513	**1/5.8**	**.051**		THR55 0.064	**1/1.6**	**.064**
41.8 (0.7)		LEU56 0.074	LEU56 0.112	**backbone**	**.186**	LEU56 0.086	LEU56 0.16	**backbone**	**.246**
32.3 (0.9)	32.4 (0.6)					LYS61 0.050	LYS61 0.104	**165/1**	**.154**

The position of each hydrogen bond is indicated by the z-position of the Cx26 atom involved (standard deviation in parentheses). Green highlight indicates residues at which hydrogen bond occupancy for the one of the test molecules was more than 0.1 greater than that for the other test molecule. Red asterisks (*) indicate for each test molecule the residues with the greatest hydrogen bond occupancy.